Biomed Microdevices (2007) 9:159–166
DOI 10.1007/s10544-006-9017-3

Solution-phase DNA mutation scanning and SNP genotyping by nanoliter melting analysis

Scott O. Sundberg · Carl T. Wittwer · Jenny Greer · Robert J. Pryor · Oluwole Elenitoba-Johnson · Bruce K. Gale

Published online: 13 December 2006

Abstract Solution-phase, DNA melting analysis for heterozygote scanning and single nucleotide polymorphism (SNP) genotyping was performed in 10 nl volumes on a custom microchip. Human genomic DNA was PCR amplified in the presence of the saturating fluorescent dye, LCGreen® Plus, and placed within microfluidic channels that were created between two glass slides. The microchip was heated at 0.1°C/s with a Peltier device and viewed with an inverted fluorescence microscope modified for photomulitiplier tube detection. The melting data was normalized and the negative first derivative plotted against temperature. Mutation scanning for heterozygotes was easily performed by comparing the shape of the melting curve to homozygous standards. Genotyping of homozygotes by melting temperature (T_m) required absolute temperature comparisons. Mutation scanning of *ATM* exon 17 and *CFTR* exon 10 identified single base change heterozygotes in 84 and 201 base-pair (bp) products, respectively. All genotypes at *HFE* C282Y were distinguished by simple melting analysis of a 40-bp fragment. Sequential analysis of the same sample on the gold-standard, commercial high-resolution melting instrument HR-1™, followed by melting in a 10 nl reaction chamber, produced similar results. DNA melting analysis requires only minutes after PCR and is a simple method for genotyping and scanning that can be reduced to nanoliter volumes. Microscale systems for performing DNA melting reduce the reagents/DNA template required with a promise for high throughput analysis in a closed chamber without risk of contamination.

Keywords DNA melting · Mutation scanning · SNP genotyping · Xurography

S. O. Sundberg (✉)
Department of Bioengineering, University of Utah,
SLC, UT 84112, USA
e-mail: scott.sundberg@m.cc.utah.edu

C. T. Wittwer · R. J. Pryor · O. Elenitoba-Johnson
Department of Pathology, University of Utah,
SLC, UT 84112, USA

J. Greer · B. K. Gale
Department of Mechanical Engineering, University of Utah,
SLC, UT 84112, USA

Introduction

Microsystem technology has generated tremendous interest recently for use in clinical diagnostics and forensics (Verpoorte, 2002). One of the most important analytical tools, the polymerase chain reaction (PCR) (Saiki et al., 1985), can amplify a short region of DNA over 10^6-fold in 10–15 min (Wittwer et al., 1990). Several groups have developed microsystems for performing PCR in nanoliter volumes (Gulliksen et al., 2004; Hühmer and Landers, 2000; Ibrahim et al., 1998; Khandurina et al., 2000; Liu et al., 2002; Yoon et al., 2002), including one group with volumes as small as 86 pl (Nagai et al., 2001). Advantages of microscale PCR include lower reagent and target DNA consumption and better heat transfer rates for faster reaction times during thermocycling. After PCR amplification, many analytical techniques are available for detecting sequence variants, including simple size separation on a gel matrix and complex mass spectrometry methods. Some of these methods have been incorporated into microsystems; for example, PCR followed by electrophoretic separation (Waters et al., 1998; Lagally et al., 2001). However, the fabrication of the chip and integration of the detection method may become complicated.

DNA melting analysis as a complement to PCR was introduced in 1997 (Ririe et al., 1997). A dye is included in

the PCR that fluoresces in the presence of double-stranded DNA, but not single-stranded DNA. After amplification, fluorescence is monitored as the double-stranded DNA product is slowly heated. When the double helix melts, fluorescence rapidly decreases. The negative first derivative of fluorescence with respect to temperature shows the melting temperature (T_m) as maxima. Recent advances in melting analysis instrumentation (Herrmann et al., 2006) and saturating DNA dyes (Wittwer et al., 2003) allow detection and genotyping of single nucleotide polymorphisms (SNPs). If the change is heterozygous, DNA heteroduplexes alter the shape of the melting curve, providing a simple method for mutation scanning (Reed and Wittwer, 2004). If the change is homozygous, the absolute temperature of the melting transition shifts (Liew et al., 2004). DNA melting analysis, when compared to existing PCR analytical techniques, is advantageous because it is less complicated, faster (less than 20 min for PCR and analysis), and prevents contamination of the sample and environment due to its closed-tube format (Zhou et al., 2004). The specific dye used determines the capabilities of the method; LCGreen® Plus detects heterozygotes well and does not inhibit PCR (Wittwer et al., 2003).

DNA melting analysis has been previously reported in microscale systems with oligonucleotides attached to the chip surface (Dodge et al., 2004). However, immobilization of oligonucleotides adds additional complexity and cost to the fabrication of the chip. Furthermore, hybridization to immobilized probes takes significantly longer than solution-phase hybridization and is limited by steric factors and mass transport conditions. By monitoring solution-phase melting analysis on a microchip, the complexity of chip fabrication and analysis time are minimized. Using custom instrumentation and microchannel chips, we demonstrate solution-phase mutation scanning and SNP genotyping in 10 nl reaction volumes using three different genomic DNA targets. To the best of our knowledge this is the first time that solution-phase DNA melting analysis has been performed in nanoliter volumes.

Materials and methods

Microchip fabrication

The microchips were manufactured using Xurography (Bartholomeusz et al., 2005). The process uses Adobe Illustrator® (Adobe, San Jose, CA) to generate the geometry of the channel structures. The output files are exported to a knife plotter (Graphtec, Irvine, CA) which cuts the channel and well structures out of a 25 μm thick, double coated tape (9019, 3M, St. Paul, MN) consisting primarily of polyethylene terephthalate (PET), a material used with PCR in previous research (Northrup et al., 1993). Input and output ports, melting analysis wells, and connecting channels were designed as shown in Fig. 1. The channels had a cross section of 175 × 25μm. The melting analysis wells had a diameter of 715 μm and a total volume of 10 nl. The patterned tape was then sandwiched between two 25 × 75 mm glass slides. One of the glass slides had 2 mm diameter holes located at the input and output ports of the channel. A NanoPort™ assembly (Upchurch Scientific, Oak Harbor, WA) was then attached to the outlet port on the glass slide with a luer lock attachment. The input port was placed 22.5 mm from the center of the DNA analysis chamber and was used for loading the sample. A syringe was connected to the luer fitting at the outlet port and was used to create a vacuum and draw the sample through the channel into the analysis chamber. Figure 2 shows a photograph of the entire assembly (A), a photograph of the 10 nl well (B), and a cross-section sketch of the assembled microchip (C).

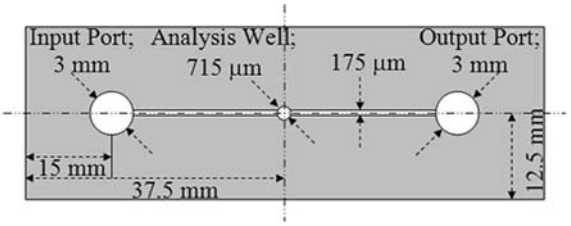

Fig. 1 Dimensioned sketch of the double coated tape cut with the knife plotter. The sketch is not to scale

Fluorescence detection

Figure 3 shows a sketch of the modified inverted microscope used for fluorescent interrogation of the microchip. For excitation, the output of a mercury arc lamp (HBO 50 W, Carl Zeiss, Thornwood, NY) was passed through two neutral density filters (ND-1, Edmund Optics, Barrington, NJ) in series to limit the light intensity, unless otherwise specified. The light passed through an excitation bandpass filter (426–446 nm, Chroma Technology Corp., Rockingham, VT), was reflected at 45° by a dichroic beam splitter (455 nm long-pass, Chroma Technology Corp.), and focused onto the analysis chamber by a 20× objective (Ph2 Achrostigmat, NA = 0.45, Carl Zeiss). Emitted light was then collected through the same lens, passed through the dichroic beam splitter and an emission bandpass filter (460–500 nm, Chroma Technology Corp.). Optic filters were designed to match LCGreen® Plus (Herrmann et al., 2006). The collimated light was focused onto the end of a fiber optic cable (400 μm diameter UV/VIS range, CVI Spectral Products, Putnam, CT) with a lens of focal length 12.6 mm and diameter 25.4 mm (AT-SHL-9, CVI Spectral Products). The fiber optic was connected to a photomultiplier tube (PMT) module (714 Photomultiplier Detection System, Photon Technology International, Birmingham, NJ) with

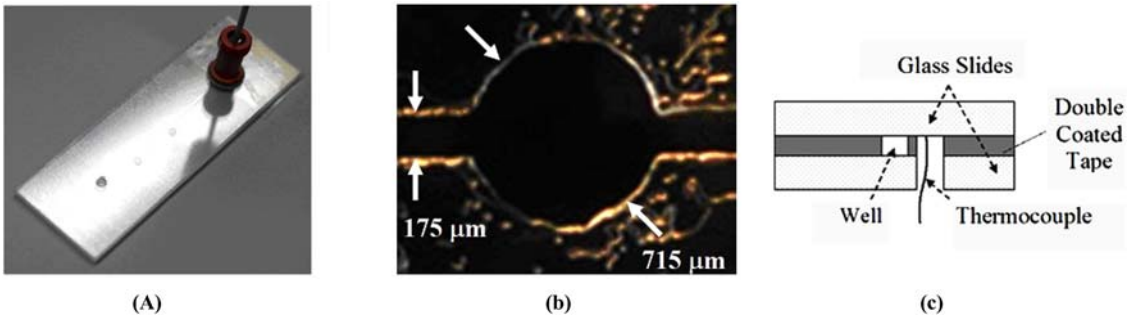

Fig. 2 (A). Photograph of the microchannel assembly with the entire chip being 25 × 75 mm. (B) Photograph of the 10 nl well with a wall height of 25 μm. (C) A cross-section sketch of the microchip at the 10 nl well. The sketch is not to scale

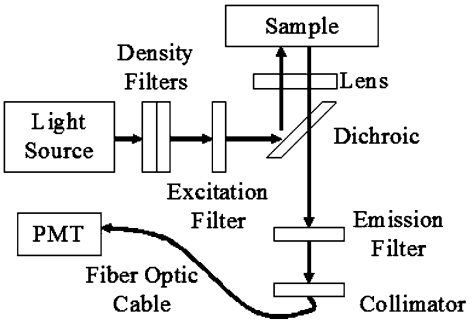

Fig. 3 Sketch of the optics set-up used in the modified inverted microscope

an R1527 PMT (Hamamatsu, Bridgewater, NJ). The analog output of the PMT module was input to a data acquisition (DAQ) card (PCI-MIO-16XE-10, National Instruments, Austin, TX) and analyzed with LabView 7.1 (National Instruments) on a personal computer. Figure 4 shows a diagram (A), and a photograph (B) of the custom system.

Temperature control

A 15 × 15 × 3.2 mm Peltier heater (TZ13153-03, Melcor, Trenton, NJ) contacted the glass slide directly above the interrogation well through a Zinc Oxide/Silicone based heat sink compound (TG-001, Melcor). A 7.5 × 3.5 × 3.5 cm steel block was placed on top of the heater as a heat sink. A J-type thermocouple (TT-J-40-50, Omega, Stamford, CT) was clamped, using a toothless alligator clip and Kapton tape, into a 2 mm diameter hole, drilled approximately 2–3 mm to the side of the analysis well, filled with heat sink compound (Fig. 2(C)). The signal from the thermocouple was amplified and linearized (AD594, Analog Devices, Norwood, MA) and the ouput was connected through a shielded I/O connector block (SCB-68, National Instruments) to the PCI-MIO-16XE-10 DAQ card. The temperature measurement was calibrated using a Fluke thermometer (54 II Thermometer, Fluke, Everett, WA) to within ±0.3°C at 50°C. Heating control was implemented using an analog output from a PCI-6014 DAQ card (National Instruments) connected to a shielded connector block (BNC-2110, National Instruments) that controlled a power supply (Zero-Up, Lamda Instruments, Neptune, NJ) connected to the Peltier device. A 550 mV input to the power supply was increased by 0.83 mV/s, resulting in a heating rate of 0.1°C/s over the temperature range of 65–85°C.

Sample preparation

Rapid cycle PCR was performed in a LightCycler® (Roche Applied Science, Indianapolis, IN) with programmed transition rates of 20°C/s. Each 10 μl mixture consisted of 50 ng of genomic DNA as the template, 0.5 μM of each primer, 200 μM of each deoxynucleotide triphosphate (dNTP), 0.4 U of KlenTaq1 polymerase (AB Peptides, St. Louis, MO), 88 ng of TaqStart antibody (ClonTech, Mountain View, CA), 2 mM $MgCl_2$, and 1 × LCGreen Plus (Idaho Technology, Salt Lake City, UT) in 50 mM Tris (pH 8.3) and 500 ng/μl bovine serum albumin (BSA). Genotyped human genomic DNA was obtained from Coriell Cell Repositories (Camden, NJ) for the *ATM* exon 17 and *HFE* C282Y DNA templates. For *CFTR* exon 10, genomic DNA was isolated and purified using the Puregene™ Genomic DNA Purification Kit (Gentra Systems, Minneapolis, MN) according to its standard protocol for 3 ml whole blood. The DNA concentration was then determined by absorbance at 260 nm (A_{260}), assuming an A_{260} of 1.0 is 50 ng/μl. The purity, according to the A_{260}/A_{280} absorption ratio, for all DNA templates was a minimum of 1.8.

Three different DNA targets were analyzed, two for mutation scanning and one for SNP genotyping. The *ATM* exon 17 PCR product (Genbank Acc.# NM 000051) (Kastan and Lim, 2000) was 84 base-pairs (bp) in length (5′-TGTCCTTTAGGGCAGCTGATATTCGGAGGAAATTG TTAAT**C**/**A**TTAATTGATTCTAGCACGCTAGAACCTAC CAAATCCCTCCACC-3′) with the SNP indicated in bold. It was amplified with primers 5′-TGTCCTTTAGGGCAGCT GAT-3′ and 5′-GGTGGAGGGATTTGGTAGGT-3′ by 30 temperature cycles of 95°C with a 0 s hold, 55°C with a 0 s hold, and 72°C with a 3 s hold.

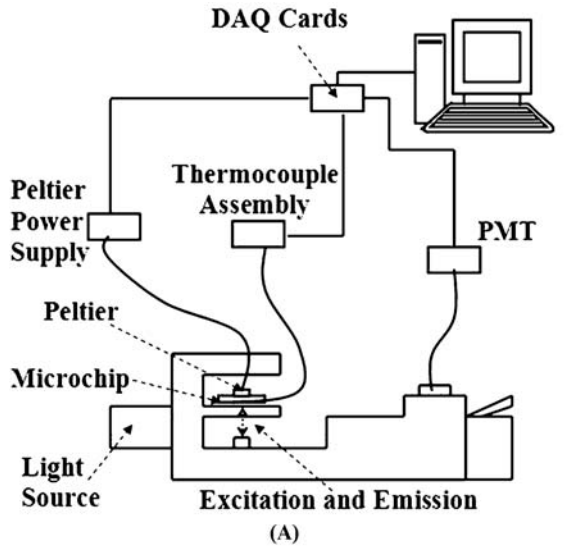

Fig. 4 (A). Diagram of the modified inverted microscope. (B) Photograph of the system with: (1) DAQ Cards; (2) Thermocouple assembly; (3) Photomultiplier assembly; (4) Microchip with thermocouple, Peltier heater, and heat sink; (5) Light source; (6) Excitation and emission filters and objective lens

The *CFTR* exon 10 PCR product (Genbank Acc.# M55115) was 201-bp in length (5′-ACTTCTAATGGTGATTATGGGAGAACTGGAGCCTTC AGAGGGTAAAATTAAGCACAGTGGAAGAATTTCA TTCTGTTCTCAGTTTTCCTGGATTATGCCTGGCACC ATTAAAGAAAATATCAT**CTT**TGGTGTTTCCTATGAT GAATATAGATACAGAAGCGTCATCAAAGCATGCCA ACTAGAAGAGGTAAGAAACTATGT-3′) with the 3-bp deletion F508del (Du et al., 2005) in bold. It was amplified with primers 5′-ACTTCTAATGGTGATTATGGG-3′ and 5′-ACATAGTTTCTTACCTCTTC-3′ after a 5 s denaturation at 95°C with 33 temperature cycles of 95°C with a 0 s hold, 54°C with a 0 s hold, and 72°C with a 4 s hold.

The *HFE* C282Y PCR product (Genbank Acc.# Z92910) (Settin et al., 2006) was 40-bp in length (5′-TGGGGAAGAGCAGAGATATACGT**G**/**A**CCAGGTGG AGCACCCA-3′) with the SNP in bold. It was amplified with primers 5′-TGGGGAAGAGCAGAGATATAC-3′ and 5′-TGGGTGCTCCACCTG-3′ after denaturation for 5 s at 95°C with 29 temperature cycles of 94°C with a 0 s hold, 55°C with a 1 s hold, and 72°C with a 1 s hold. For melting analysis of C282Y, one of the ND = 1.0 filters was replaced with a ND = 0.5 filter.

Microchip preparation

In order to prevent cross-contamination between samples, the microchannels were cleansed with DNA Away™ (Molecular BioProducts, San Diego, CA), flushed with DI water, and then coated with BSA (Al-Soud and Radstrom, 2001), at a concentration of 2.5 mg/ml, before each run. One channel was used for all genotypes of *ATM* exon 17 and one channel was used for *HFE* C282Y targets, allowing optimal temperature reproducibility between genotypes. *CFTR* exon 10 used two chips, one for each of the genotypes tested.

Melting curve acquisition and analysis

After amplification, the LightCycler capillary was transferred to an HR-1™ instrument (Idaho Technology) and heated at 0.1°C/s for a high-resolution reference melting curve. The sample was then spun out of the capillary into a microfuge tube and one μl of sample was injected into the channel inlet port using a micro-pipette. A syringe on the outlet port was used to pull the sample into the channel. The *x* and *y*-axis stage of the inverted fluorescent microscope (Axiovert 100, Carl Zeiss) was used to align the 10 nl well with the optics and the *z*-axis was used for focus. The sample was heated at 0.1°C/s with 20 data points acquired every 1°C. At least three melting curves were obtained for each genotype.

HR-1 and microchip melting data were analyzed using custom software written in LabView as previously described (Gundry et al., 2003; Wittwer et al., 2003). Fluorescence intensity values were normalized between 0 and 100% by defining linear baselines before and after the melting transition of each sample. Negative derivative plots for each curve were calculated using Savitsky-Golay (Press et al., 1992) polynomials of the second-degree at each point with a 33–40 point window for the microchip data. For data from the HR-1, a window of 60–90 points was used. The normalized melting curves reported for *CFTR* exon 10 had the temperature axis of each curve adjusted to superimpose each of the curves over a specified fluorescence interval, as described previously (Wittwer et al., 2003). Temperature axis adjustment allowed shape distinction between the two genotypes

tested. Signal-to-noise ratios (S/N) were calculated, as described previously (Herrmann et al., 2006).

Results and discussion

Solution-phase mutation scanning and SNP genotyping with DNA dyes can be performed within a microchip at a thousand-fold reduction in analysis volume from current systems. Complete genotyping at the C282Y locus was achieved with both homozygotes and the heterozygote easily differentiated. For scanning, a SNP heterozygote was detected within *ATM* exon 17 and a 3-bp deletion within *CFTR* exon 10. Mutation scanning is a process used to scan for mutations within a targeted region of DNA. Heterozygotes were easily identified for the known targets analyzed. Further study of previously unknown mutations would be necessary to establish the sensitivity and specificity of the method. These methods do not require any sample processing, electrophoretic separation, labeled probes, real-time PCR or allele-specific amplification.

Figure 5 shows derivative melting plots of normal and heterozygous DNA for a SNP within an 84-bp fragment of *ATM* exon 17. Panel (A) shows results from a 10 nl sample using the microchip system, in good agreement with panel (B), the HR-1 instrument with a 10 μl sample volume. The HR-1 instrument is the gold standard for high-resolution melting analysis with an absolute temperature standard deviation $< 0.02^{\circ}$C and 200 data points for every 1°C (Herrmann et al., 2006). In both systems, there is a clear distinction between heterozygous and homozygous products, observed as a change in curve shape. This shape change occurs because of the contribution of heteroduplexes to the overall melting curve as previously described (Gundry et al., 2003; Wittwer et al., 2003). Similarly, Fig. 6 shows ten derivative melting plots of both normal and heterozygous DNA for a 3-bp deletion within a 201-bp fragment of *CFTR* exon 10. The 10 nl volume plot (A) again shows good agreement with the 10 μl plot (B) and in both instruments, heterozygotes are clearly identified. The normalized and temperature axis adjusted melting curves showed a distinction by shape of the normal and heterozygous samples within the 10 nl plot (C) and the 10 μl plot (D). It is noted that the temperature variation between chips is large for this target yet the shape of the curves were all distinguishable, thus allowing correct detection of mutations for the 20 samples analyzed.

Figure 7 shows full genotyping at the C282Y locus of *HFE*. Again, the microchip data in (A) is very similar to the HR-1 data in (B). Heterozygous melting curves show the characteristic shape change resulting from heteroduplexes. Wild-type and mutant homozygotes are distinguished by their T_ms, with the mutant allele about 2°C lower than the wild-type allele.

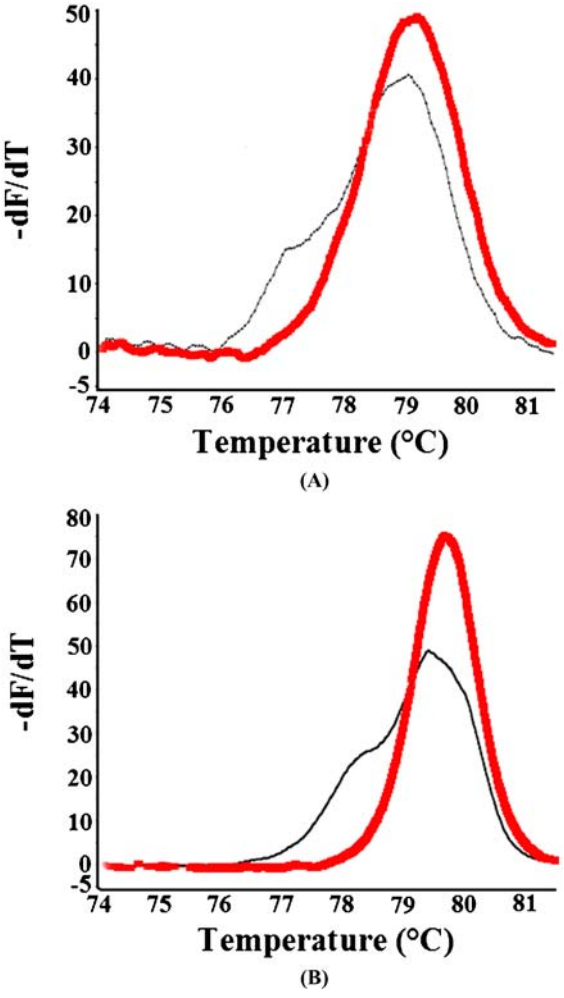

Fig. 5 Negative derivative plots for the microchip (A: 10 nl) and the HR-1 (B: 10 μl) using the *ATM* exon 17 target. Homozygous wild-type template (*red line*); heterozygous mutant template (*black line*)

Table 1 lists the S/N and T_ms for each genotype in both instruments. Even though the reaction volume is decreased by three orders of magnitude, the S/N for the microchip is only 1.5 orders of magnitude less than that of the HR-1. As can be seen from Figs. 5–7, the microchip S/N is adequate for both mutation scanning and genotyping. T_ms were similar on both instruments, although differences between 0.2–1.6°C were observed. These shifts were specific to each microchip studied and are explained by the thermal gradient across the Peltier heater (0.3–0.4°C/mm) and variation in the thermocouple placement relative to the analysis well (0.1–0.4 mm). A larger Peltier device and/or addition of a conducting plate between the heater and the melting chip should distribute heat more evenly. Broader melting transitions of the negative derivative plots were observed on the microchip relative to the HR-1 (Figs. 5–7). This broadening is an artifact of the Savitsky–Golay polynomials, due to the fact that fewer points were fitted for the microchip plots.

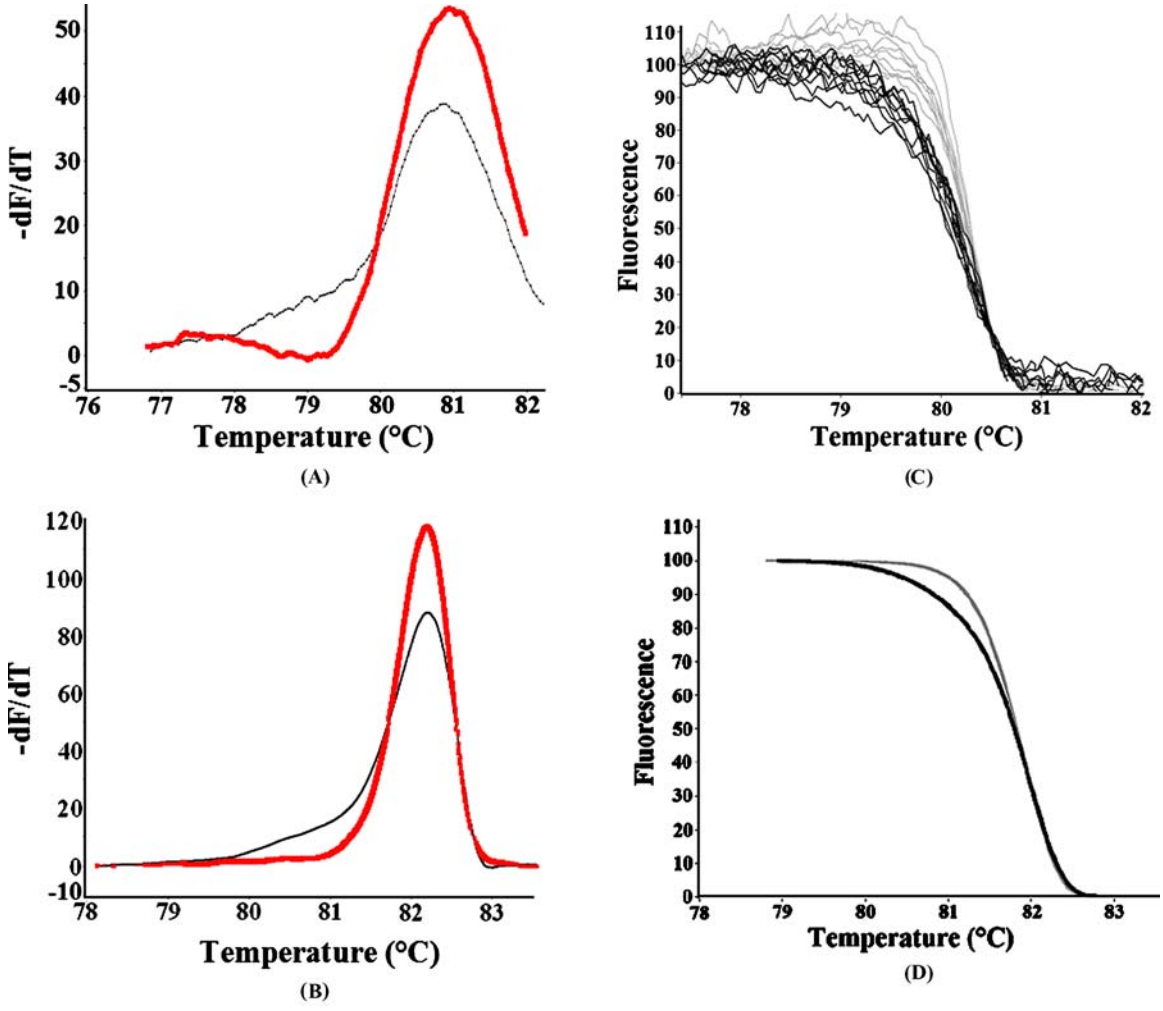

Fig. 6 Negative derivative plots for the microchip (A: 10 nl) and the HR-1 (B: 10 μl) using the *CFTR* exon 10 target. Homozygous wild-type template (*red line*); heterozygous mutant template (*black line*). Normalized and temperature axis shifted melting plots for the microchip (C: 10 nl) and the HR-1 (D: 10 μl) using the *CFTR* exon 10 target. Homozygous wild-type template (*gray lines*); heterozygous mutant template (*black lines*)

Figure 6(C) and (D) indeed show that the slopes of the melting curves between the microchip and HR-1 are very similar.

The Xurography microchip manufacturing process was appealing because it did not require clean room techniques, thus lowering manufacturing costs, and the fabrication was quite rapid (a microchip could be built and DNA tests performed within a working day). One other group has previously reported the use of this manufacturing technique, fabricating a DNA extraction microchip (Kim et al., 2005). Using Xurography, a microchip channel design was cut out of an adhesive-backed plastic and placed within a Petri dish to create a polydimethylsiloxane (PDMS) mold. The method used here is even simpler because no further fabrication processes are required beyond Xurography.

The standard mercury light source in the microscope was far too bright when focused on the sample, causing rapid photobleaching. Neutral density filters were used to reduce the excitation intensity and better match the fluorescence emission to the photomultiplier detector used. Alternative light sources, such as high intensity LEDs to flood illuminate a small area without precise focusing are interesting options. Furthermore, a charge-coupled-device (CCD) camera could image a DNA melting array microchip, thereby creating a higher throughput system. CCDs, although not as sensitive as PMTs, should provide sufficient S/N for nanoliter volume melting of amplified DNA.

Conclusion

Solution-phase DNA melting analysis for mutation scanning and genotyping can be performed in 10 nl reaction chambers within a microchip. The 1000-fold reduction in sample volume from 10 μl in state-of-the art commercial systems to

Table 1 Signal-to-noise (S/N) and melting temperatures (T_ms) of seven genotypes at three loci on the HR-1 (10 μl) and microchip (10 nl) instruments

	S/N		T_m (°C)		
	HR-1	Microchip[a]	HR-1	Microchip[b]	ΔT_m[c]
ATM exon 17					
Homozygous wild-type	2450	69	79.7	78.8 ± 0.7	0.9
Heterozygous mutant	2800	63	79.5	78.1 ± 0.8	1.4
CFTR exon 10					
Homozygous wild-type	5000	168	82.4	80.7 ± 0.5	1.7
Heterozygous mutant	5350	135	82.4	79.9 ± 0.3	2.5
HFE C282Y					
Homozygous wild-type	2680	76	79.6	79.4 ± 0.6	0.2
Heterozygous mutant	2290	60	78.4	77.8 ± 0.7	0.6
Homozygous mutant	2560	111	77.9	77.5 ± 0.5	0.4

[a]Microchip S/N values are averaged over 3 unique melt curves for each genotype of *ATM* exon 17 and *HFE* C282Y. *CFTR* exon 10 represents averaged values over ten unique melt curves for each genotype.

[b]Microchip T_m reports the average value over three melts for *ATM* exon 17 and *HFE* C282Y targets and an average value over ten melts for *CFTR* exon 10 with the standard deviation.

[c]Values represent the difference between the HR-1 T_m and the averaged Microchip T_m.

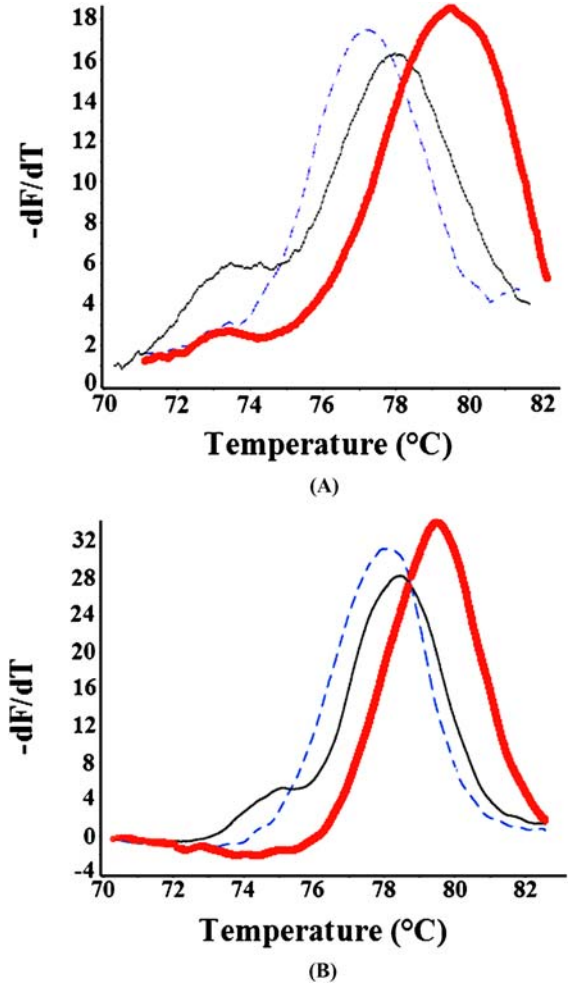

Fig. 7 Negative derivative plots for the microchip (A: 10 nl) and the HR-1 (B: 10 μl) using the *HFE* C282Y target. Homozygous wild-type template (*red line*); heterozygous mutant template (*black line*); homozygous mutant template (*blue dashed line*)

10 nl on the microchip does result in a lower S/N, but is entirely adequate for detecting and genotyping SNPs. Mutation scanning was performed in 84 and 201-bp PCR products, and complete SNP genotyping by melting a 40-bp target. The characteristic features of the melting curves necessary for scanning and genotyping are produced by both the nl microchip and the μl commercial instrument. The next logical step is to integrate PCR with melting analysis on the microchip, potentially in an array format. Such a system would be relatively easy to fabricate and could provide a rapid, inexpensive, high-throughput mutation scanning and genotyping solution that requires no separations, processing, or labeled probes.

Acknowledgments This work was funded by State of Utah Center of Excellence grants for Biomedical Microfluidics and for Homogeneous DNA Melting Analysis, and NSF IGERT grant number DGE-9987616. We thank Luming Zhou and Gudrun Reed for providing samples and PCR protocols for the *ATM* exon 17 and *CFTR* exon 10 targets. We also thank Dr. Wittwer's lab group and Dr. Gale's lab group for valuable advice pertaining to this research.

References

W.A. Al-Soud and P.J. Radstrom, Clin. Microbiol. **39**(2), 485–493 (2001).

D.A. Bartholomeusz, R. Boutté, and J.D. Andrade, J. MEMS **14**, 1364–1374 (2005).

A. Dodge, G. Turchatti, I. Lawrence, N.F. de Rooij, and E. Verpoorte, Anal. Chem. **76**, 1778–1787 (2004).

K. Du, M. Sharma, and G.L. Lukacs, Nat. Struc. Mol. Biol. **12**(1), 17–25 (2005).

A. Gulliksen, L. Solli, F. Karlsen, H. Rogne, E. Hovig, T. Nordstrom, and R. Sirevåg, Anal. Chem. **76**, 9–14 (2004).

C.N. Gundry, J.G. Vandersteen, G.H. Reed, R.J. Pryor, J. Chen, and C.T. Wittwer, Clin. Chem. **49**(3), 396–406 (2003).
M.G. Herrmann, J.D. Durtschi, L.K. Bromley, C.T. Wittwer, and K.V. Voelkerding, Clin. Chem. **52**, 494–503 (2006).
A.F.R. Hühmer and J.P Landers, Anal. Chem. **72**, 5507–5512 (2000).
M.S. Ibrahim, R.S. Lofts, P.B. Jahrling, E.A. Henchal, V.W. Weedn, A. Northrup, and P. Belgrader, Anal. Chem. **70**, 2013–2017 (1998).
M.B. Kastan and D.S. Lim, Nat. Rev. Mol. Cell Biol. **1**, 179–186 (2000).
J. Khandurina, T.E. McKnight, S.C. Jacobson, L.C. Walters, R.S. Foote, and J.M. Ramsey, Anal. Chem. **72**, 2995–3000 (2000).
J. Kim, K.V. Voelkerding, and B.K. Gale, in 3rd Annual International IEEE EMBS Special Topic Conference on Microtechnologies in Medicine and Biology, Kahuku, Oahu, HI, (May 12–15, 2005), pp. 5–7.
E.T. Lagally, C.A. Emrich, and R.A. Mathies, Lab on a Chip **1**, 102–107 (2001).
M. Liew, R. Pryor, R. Palais, C. Meadows, M. Erali, E. Lyon, and C. Wittwer, Clin. Chem. **50**(7), 1156–1164 (2004).
J. Liu, M. Enzelberger, and S. Quake, Electrophoresis **23**, 1531–1536 (2002).
H. Nagai, Y. Murakami, Y. Morita, K. Yokoyama, and E. Tamiya, Anal. Chem. **73**, 1043–1047 (2001).
M.A. Northrup, M.T. Ching, R.M. White, and R.T. Watson, Transducers **93**, 924–927 (1993).
W.H. Press, S.A. Teukolsky, W.T. Vetterling, and B.P. Flannery, Numerical Recipes in C, 2nd ed. (Cambridge University Press, New York 1992), pp. 650–655.
G.H. Reed and C.T. Wittwer, Clin. Chem. **50**(10), 1748–1754 (2004).
K.M. Ririe, R.P. Rasmussen, and C.T. Wittwer, Anal. Biochem. **245**, 154–160 (1997).
R.K. Saiki, S. Scharf, F. Faloona, K.B. Mullis, G.T. Horn, H.A. Erlich, and N. Arnheim, Science **230**, 1350–1354 (1985).
A. Settin, M. El-Bendary, R. Abo-Al-Kassem, and R. El Baz, J Gastrointestin Liver Dis. **15**(2), 131–135 (2006).
E. Verpoorte, Electrophoresis **23**, 677–712 (2002).
L.C. Waters, S.C. Jacobson, N. Kroutchinina, J. Khandurina, R.S. Foote, and J.M. Ramsey, Anal. Chem. **70**, 5172–5176 (1998).
C.T. Wittwer, G.C. Fillmore, and D.J. Garling, Anal. Biochem. **186**(2), 328–331 (1990).
C.T. Wittwer, G.H. Reed, C.N. Gundry, J.G. Vandersteen, and R.J. Pryor, Clin. Chem. **49**(6), 853–860 (2003).
D.S. Yoon, Y. Lee, Y-S. Lee, Y. Lee, H.J. Cho, S.W. Sung, K.W. Oh, J. Cha, and G.J. Lim, Micromech. Microeng. **12**, 813–823 (2002).
L. Zhou, A.N. Myers, J.G. Vandersteen, L. Wang, and C.T. Wittwer, Clin. Chem. **50**(8), 1328–1335 (2004).